International Journal of Mass Spectrometry 285 (2009) 49–57

Contents lists available at ScienceDirect

International Journal of Mass Spectrometry

journal homepage: www.elsevier.com/locate/ijms

Fractionation and mixing in a thermal ionization mass spectrometer source: Implications and limitations for high-precision Nd isotope analyses

Rasmus Andreasen[a,b,*], Mukul Sharma[a]

[a] Radiogenic Isotope Geochemistry Laboratory, Department of Earth Sciences, Dartmouth College, 6105 Sherman Fairchild Hall, Hanover, NH 03755, USA
[b] Department of Earth Science & Engineering, Imperial College London, South Kensington, London SW7 2AZ, United Kingdom

ARTICLE INFO

Article history:
Received 19 December 2008
Received in revised form 9 April 2009
Accepted 10 April 2009
Available online 19 April 2009

Keywords:
Thermal ionization mass spectrometry
Neodymium
Mass fractionation
Exponential law
Rayleigh law

ABSTRACT

We present a large dataset of normal Nd standard analyses to evaluate the adequacy of commonly used "laws" to correct for the mass dependent isotope fractionation introduced in a thermal ionization mass spectrometer (TIMS) source, and to assess if the assumption of homogenous sample evaporation and ionization from one sample domain on the filament can be considered valid when obtaining high precision (better than 5 ppm, 2σ) $^{142}Nd/^{144}Nd$ ratios for studies in geo- and cosmochemistry. The exponential law is fully adequate to correct for the mass fractionation at the current level of obtainable precision and surprisingly performs better than the Rayleigh law. Our modelling shows that the observed correlations in the isotope ratios that remain after data have been corrected using the exponential law are a consequence of correlated uncertainties in counting statistics. These correlations are therefore not from residuals resulting from inadequate correction. Application of the exponential law, however, assumes evaporation from a single homogenous domain on the filament—a condition which was impossible to maintain even under optimal sample loading and heating conditions. While a majority of samples showed an increase in heavy/light isotope ratio with time (normal fractionation), many samples showed the reverse trend (reverse fractionation) indicating evaporation and mixing from variably depleted domains on the filament. Our modelling suggests that up to 50% of the calculated external reproducibility (=standard deviation of the population, σ_p of n independent measurements) can be explained by the ion emission from multiple domains of somewhat different isotopic composition on the filament. The fractionation behaviour of a sample is not necessarily a good indicator of the extent of domain mixing as mixing effects in data collected during reverse fractionation are similar to those of data collected during normal fractionation before and after periods of reverse fractionation. Domain mixing effects in $^{142}Nd/^{144}Nd$ isotope ratios can be assessed by examining variations in stable $^{148}Nd/^{144}Nd$ and $^{150}Nd/^{144}Nd$ ratios. The ^{148}Nd and ^{150}Nd data from recent reports of ^{142}Nd deficits in terrestrial samples suggest that the ^{142}Nd anomalies are likely produced from domain mixing during analysis rather than from the decay of short-lived ^{146}Sm during the early history of the earth. It is imperative to measure all the isotopes of Nd to the utmost possible precision and to examine domain mixing effects by normalizing the data using multiple isotope pairs.

1. Introduction

The intent of this study is to evaluate the extent to which the accuracy of highly precise measurements of Nd isotope ratios is affected by our lack of understanding of the mass dependent isotope fractionation and mixing that takes place in the mass spectrometer source during analysis. Recent improvements in multi-collector thermal ionization mass spectrometry have renewed interest in the coupled ^{146}Sm–^{142}Nd and ^{147}Sm–^{143}Nd radioactive decay system as a chronometer for early silicate differentiation within planetary bodies [1–10]. The new generation mass spectrometers (mainly ThermoFinnigan Triton) have minimized sources of random errors and systematic bias during analysis (see [11,12] for a complete discussion of uncertainties). These improvements have permitted routine measurements of Nd isotope ratios with an external reproducibility (=standard deviation of the population, σ_p of n independently loaded standards) that is similar in magnitude to the internal precision (=standard error, σ_m) of a single standard. However, repeated measurements of rock samples, in general, display isotope variations that are much larger than expected from repeated analyses of standards (cf. [9]). Since Nd standards are solutions of metal salts with a matrix that is likely different from Nd separated

* Corresponding author at: Department of Earth Science & Engineering, Imperial College London, South Kensington, London SW7 2AZ, United Kingdom.
Tel.: +44 0 20 7594 6474; fax: +44 0 20 7594 7444.
E-mail address: r.andreasen@imperial.ac.uk (R. Andreasen).

1387-3806/$ – see front matter © 2009 Elsevier B.V. All rights reserved.
doi:10.1016/j.ijms.2009.04.004

from rocks, the above observation suggests that differences in the evaporation and fractionation behaviour of Nd in the mass spectrometer between standards and samples and between different samples impacts our ability to resolve small variations in Nd isotope ratios.

In the source of a thermal ionization mass spectrometer (TIMS), a solid sample is evaporated and ionized. The evaporation favours lighter species, relative to heavier; as evaporation progresses, a sample becomes relatively depleted in lighter isotopes, resulting in decreasing light/heavy isotope ratios during analysis. To correct for the mass fractionation a number of empirical fractionation "laws" (most notably the linear, power, and exponential laws) [13,14] have been developed over the years, in addition to the theoretically based Rayleigh law, which describes diffusion and evaporation in vacuum [15,16]. Of the empirically derived fractionation laws, the linear and power laws have been shown to be insufficient in effectively correcting for mass fractionation, over the mass range of Nd [17,18], such that fractionation-correcting a given dataset leaves correlations between measured and fractionation-corrected isotope ratios, whereas the commonly used exponential law and the more mathematically complex Rayleigh law have been found to correct for mass fractionation more accurately (cf. [2]). Correlations between fractionation-corrected ratios of lighter and heavier isotopes are still present and have been used to implement secondary mass fractionation corrections [1,19,20] While some of the correlations have been found to be caused by ion optical aberrations induced by the introduction of a magnet in the ion source [1,4] and others have been thought to stem from fractionation and mixing in the ion source [2], the key issue still remains is the extent to which fractionation laws may be used to obtain precise and accurate isotope ratios.

All fractionation laws require the assumption that sample evaporation takes place from a single, homogenous domain on a filament. This assumption is probably not justified, as mass fractionation is temperature dependent, and the temperature across a sample-laden filament may not be the same, even if the sample is loaded in a small, well-defined area whose diameter is $\leq$1 mm. This is especially true when only a fraction of a large sample loaded on the filament is sufficient to provide the ion beam of required intensity. Hart and Zindler [21] have shown that for an equal-abundance isotope mixture of calcium, an ion beam is derived from sample domains that are depleted to differing extents. Recently, this has also been reported for Nd [2,22].

For this reason, we wish to evaluate: (i) The nature of mass fractionation in a thermal ionization mass spectrometer source, (ii) the ability of the Rayleigh law and the empirically derived fractionation laws to correct for such mass dependent fractionation, (iii) the extent to which an ion beam represents multiple sample domains, having differing isotopic compositions, on a filament; and if domain mixing does occur, and (iv) the effect that such mixing has on high-precision, high-accuracy Nd isotopic measurements. To this end, we present an extensive dataset of more than 200 isotopic measurements of the Caltech nNd-β neodymium standard measured over a period of nearly 3 years. Finally, we examine Nd isotopes in some recently published rock data to assess the extent to which they have been impacted by domain mixing.

2. Methods

The Nd standard data obtained in this study was acquired under three different mass spectrometry conditions on the Dartmouth Triton TIMS (cf. [9]). These temporally distinct conditions are labelled Stages 1, 2, and 3. For all three stages the same filament loading procedure was used: $NdCl_3$ was sandwiched between dilute H_3PO_4. Approximately 0.5 μl of 0.01 M H_3PO_4 was loaded on a zone refined Re filament (H. Cross) and dried at 0.8 A. Next about 250–300 ng of Nd dissolved in 1 μl of 2.5 M HCl was loaded and dried. Finally, 0.5 μl of 0.01 M H_3PO_4 was loaded and dried and the filament current raised slowly to 1.8 A and kept there for 6 s. The filament with sample (evaporation filament) was put in a double filament assembly with a blank Re filament (ionization filament). The sample size was chosen as to optimize the relationship between ion beam intensity, extent of fractionation, and measurement duration, allowing for a stable ion beam of ~50 pA of ^{144}Nd, for a period of ~2 h. This gave average measured ^{146}Nd/^{144}Nd values straddling around the consensus value of 0.7219 used for fractionation correction, so that all analyses are close to optimal fractionation. Equivalent counting statistic uncertainty calculations suggest that an internal $2\sigma_m$ precision of ~2.5 ppm in addition to ~0.3 ppm uncertainty from the Faraday cup baselines should be the limit for these measurements. For measurements during Stage 1, the evaporation filament was heated higher than the ionization filament as this improved ionization efficiency by a factor of two compared to the traditional way of predominantly heating the ionization filament [10]. For Stages 2 and 3 the traditional approach was followed despite the lower ionization efficiency (~1%) as this gave a more stable ion emission.

During analyses in Stage 1, all 7 Nd isotopes were measured simultaneously in static multi-collector mode (Table 1). A total of 9 data blocks were collected, each block consisting of 20 integration cycles of 8 s. Amplifier gain biases and their uncertainties were cancelled by sequentially rotating the amplifier-Faraday cup connections between blocks. Faraday baseline measurements were obtained prior to each block by deflecting the beams before the magnet, at the exit from the source. Isobaric interferences on ^{142}Nd (from ^{142}Ce), ^{144}Nd, ^{148}Nd, and ^{150}Nd (from ^{144}Sm, ^{148}Sm, and ^{150}Sm, respectively) were monitored using intensities of ^{140}Ce and ^{147}Sm determined by a secondary electron multiplier (SEM) operating in ion counting mode immediately before and after each Nd measurement. Cerium interferences on ^{142}Nd are less than 0.5 ppm, samarium interferences on ^{144}Nd are ~0.1 ppm. All isobaric interferences are negligible and no interference corrections were done.

Following a major service/upgrade of the mass spectrometer in the spring of 2005 that involved replacement of the collectors used for multi-ion counting (channeltrons), a leaky gate valve, and the SEM electronics, the external reproducibility of Nd isotope ratios degraded significantly. Recognizing that the data quality was being affected by variable cup collector efficiencies, a dynamic double-jump mode of data collection and reduction procedure was developed that cancelled out differences in cup collector efficiencies and permitted high-precision ^{142}Nd/^{144}Nd ratio measurements. This configuration (Stage 2) uses only the centre cup and the low- and high-mass cups immediately adjacent to the centre cup. Following measurement of ^{140}Ce; ^{142}Nd; and ^{144}Nd the magnetic field was switched to measure ^{142}Nd; ^{144}Nd; and ^{146}Nd (jump 1), and then ^{144}Nd; ^{146}Nd; and ^{148}Nd (jump 2) (Table 1). The geometry of the Triton does not permit complete overlapping of ion-peaks when the magnetic field is switched. This was accomplished by changing the dispersion of the ion-beams with a quadrupole ("zoom focusing"). Data were collected for 15 blocks, each block containing 10 cycles that, in turn, consisted of 8 s of integration time. Faraday baselines were measured for 30 s at the beginning of every block and amplifier connections were rotated between blocks. Interferences of ^{142}Ce on ^{142}Nd are ~0.5 ppm, well within the internal precision. Nonetheless all data obtained in Stage 2 are Ce-corrected. Isobaric interferences of Sm on ^{144}Nd and ^{148}Nd were measured directly before and after data acquisition, Sm interference was ~0.1 ppm on ^{144}Nd and no correction for Sm interference was done.

The problem of variable cup collection efficiencies was eliminated in October 2005 when new graphite inserts for all the Faraday cups were installed. Subsequently, static multi-collector mode was employed again in Stage 3. Data were collected for 15 blocks, each

Table 1
Faraday cup configurations used for the Nd isotope measurements.

L3	L2	L1	Ax	H1	H2	H3
Static measurements: Stages 1 and 3						
^{142}Nd	^{143}Nd	^{144}Nd	^{145}Nd	^{146}Nd	^{148}Nd	^{150}Nd
		L1	Ax	H1		
Dynamic measurements: Stage 2						
Jump 1		^{140}Ce	^{142}Nd	^{144}Nd		
Jump 2		^{142}Nd	^{144}Nd	^{146}Nd		
Jump 3		^{144}Nd	^{146}Nd	^{148}Nd		

block comprising 14 cycles of 16 s integration. Faraday baselines were measured for 30 s before every block and the amplifier connections rotated between blocks. Isobaric interferences are similar to Stage 1 and no corrections were made.

3. Results and discussion

The Caltech nNd-β standard was measured 77 times during Stage 1, 74 times during Stage 2, and 53 times during Stage 3, giving 2645 data blocks—37,395 individual measurements. The average values of the standard measurements are given in [9]; a subset of Stage 1 is given in [2]. For the purpose of the present study statistical calculations on the entire standard population are performed in order to investigate the fractionation behaviour and extent of domain mixing. This approach deviates from the traditional method of examining individual standard runs in details, but is done in order to have a sufficiently large dataset to quantify systematic behaviour better than what can be done based on single measurements.

To evaluate the fractionation behaviour of the standard, the measured ^{142}Nd/^{144}Nd and ^{150}Nd/^{144}Nd ratios from Stage 1 are shown in Fig. 1 along with calculated trajectories of commonly used mass fractionation laws. The data from Stage 1 was chosen as it shows the largest variations in measured Nd isotope ratios and ^{142}Nd and ^{150}Nd, the lightest and heaviest Nd isotopes respectively show the largest mass dependent fractionation effects. As can be seen in the magnified insets of high ^{142}Nd/^{144}Nd & low ^{150}Nd/^{144}Nd, and low ^{142}Nd/^{144}Nd & high ^{150}Nd/^{144}Nd the data the linear, power, and linearized Raleigh laws do not provide good approximations to the data at when data are highly under- or overfractionated (i.e., when $|F| > 0$, F being defined as the deviation in fractionation from the 'true' ^{146}Nd/^{144}Nd ratio of 0.7219 used for mass dependent fractionation correction per atomic mass unit

$$\%F = [(^{146}\mathrm{Nd}/^{144}\mathrm{Nd}_{\mathrm{Meas.}}/0.7219 - 1)/(m_{^{146}\mathrm{Nd}} - m_{^{144}\mathrm{Nd}})] \times 100$$

all the fractionations laws converge at $F = 0$). This deviation from the power and linear laws is long established [17,18]. More importantly the Rayleigh law and in particular the exponential law seem to be able to account for the mass dependent fractionation introduced in the mass spectrometer source.

The ^{150}Nd/^{142}Nd ratio, display the largest mass range of the Nd isotope ratios (8 amu or 5.6%), and thus provide the best test of fractionation laws. In Fig. 2 the deviation from Rayleigh law behaviour in parts per million as a function of measured ^{146}Nd/^{144}Nd ratio is shown for all data blocks of the nNd-β standard measured during Stages 1 and 3. It is evident, despite the relatively large uncertainties, that there is clear dependency between the degree of fractionation and the Rayleigh law corrected data. The exponential law provides a better fit to the data and does not deviate significantly from the best-fit line (York-fit, Isoplot [23]). The exponential law therefore performs the most accurate correction for mass dependent Nd isotope fractionation. For the range of *F*-values observed here (−0.17 to +0.19% amu^{-1}) the exponential law correction produces no significant trends for *all* Nd isotope ratios. However, trends are present among exponential law corrected Nd

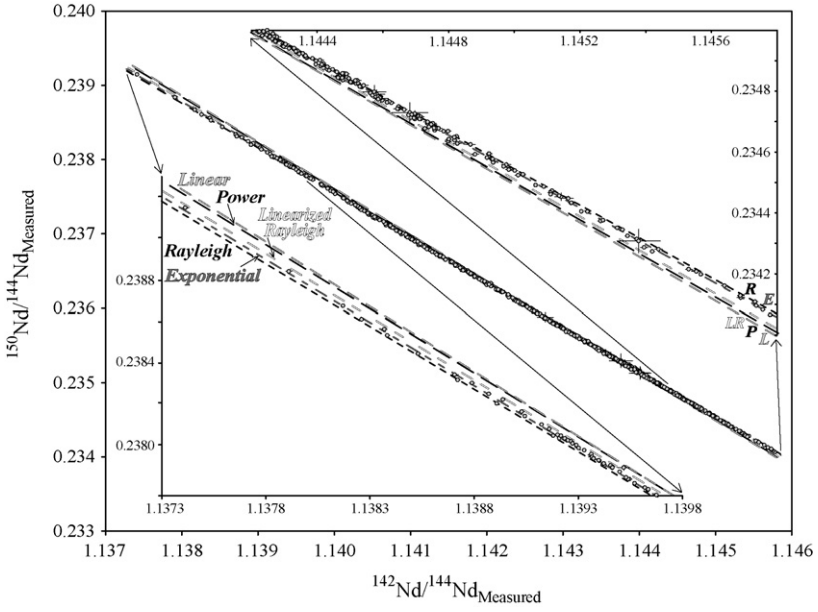

Fig. 1. Measured ^{150}Nd/^{144}Nd against measured ^{142}Nd/^{144}Nd for the 795 data blocks from Stage 1 along with calculated trajectories for various fractionation laws: linear law (*L*), power law (*P*), linearized Rayleigh law (*LR*), exponential law (*E*), and Rayleigh law (*R*). Inserts show the underfractionated and overfractionated ends where the fractionation laws deviate.

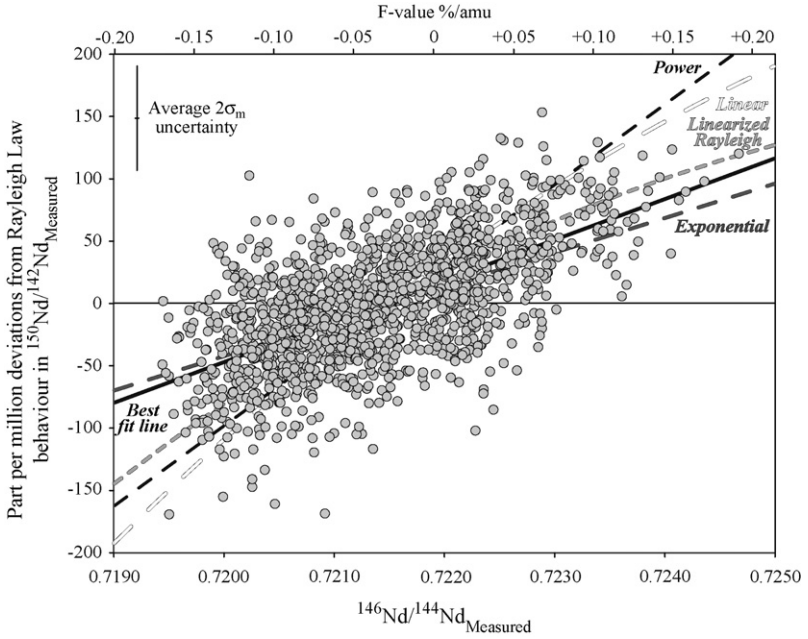

Fig. 2. Deviation in measured $^{150}Nd/^{142}Nd$ from Rayleigh law behaviour against measured $^{146}Nd/^{144}Nd$ for data blocks from Stages 1 and 3, along with a best-fit line (BF) and calculated trajectories for the: linear-, power-, linearized Rayleigh-, and exponential laws. For clarity the average $2\sigma_m$ is shown instead of individual error bars.

isotope ratios. Previous studies [1,19,20] have assumed that these trends have resulted from insufficient mass bias correction by the exponential law and have suggested (empirical) secondary mass-dependent correction. Although the trends observed in one of the above studies [1] were later identified to be due to ion-optical aberrations [4], the reasons behind the correlated variations among the exponential law corrected Nd isotope ratios remain unclear. The key issue is whether the observed trends are indeed the result of the application of an improper fractionation correction or whether they are caused by correlated errors in counting statistics. We investigate this issue below with the aid of a model (Table 2).

Fig. 3 shows the correlations in Nd isotope ratios for all individual ratios of the nNd-β standard *measured* during Stage 3 (n = 10,770) in the upper right hand panel, and the same number of *modelled* isotope ratios in the lower left panel. The real data were acquired over a range of F-values—from −0.16% to +0.08%, with an average of −0.02%, whereas the modelled data are obtained at an F-value of 0, in order to examine the effect of fractionation. The model includes an estimate of the uncertainty in the ion beam intensity with a Gaussian distribution around of $1/\sqrt{N}$ (Table 2). There is a positive correlation between ratios of two isotopes that are either both lighter or both heavier than the normalizing isotopes ^{144}Nd and ^{146}Nd (e.g., μ^{142}_{Nd} vs. μ^{143}_{Nd} and μ^{148}_{Nd} vs. μ^{150}_{Nd}), and a negative correlation between ratios of isotopes where one is heavier and one, lighter than the normalizing isotopes. Variations in ^{145}Nd do not correlate with variations in any of the other Nd isotopes. The slope of the best-fit line of each of the real, correlated data could suggest mass dependent relationships introduced by the fractionation correction, but it is difficult to establish a consistent trend that describes the relationships between all isotope pairs. The slopes of the best-fit lines between μ^{142}_{Nd} vs. μ^{148}_{Nd} and μ^{142}_{Nd} vs. μ^{150}_{Nd} are, for example, the same as those of the best-fit lines between μ^{143}_{Nd} vs. μ^{148}_{Nd} and μ^{143}_{Nd} vs. μ^{150}_{Nd}. The scatter in the modelled data is slightly smaller than that in the measured data; more importantly the slopes of the best-fit lines for a given isotope pair are the same within error for the real and the modelled data. As the model data are generated at a constant F-value of 0, the above observation indicates that the trends do not result from incorrect mass fractionation correction. This further suggests that the correlations in the mass fractionation corrected data are due to correlated counting statistical errors, and are not introduced during the mass fractionation correction calculations.

This issue can be explored further by comparing the $^{142}Nd/^{144}Nd$ and $^{148}Nd/^{144}Nd$ data collected in static mode during Stage 3, with the $^{142}Nd/^{144}Nd$ and $^{148}Nd/^{144}Nd$ data collected in dynamic mode during Stage 2. In static mode, all isotopes of Nd are measured simultaneously, whereas in dynamic mode, a subset of isotopes is measured at any given time. The dynamic setup used during Stage 2 (Table 1) measured ^{142}Nd; ^{144}Nd; and ^{146}Nd in the second cycle, and ^{144}Nd; ^{146}Nd; and ^{148}Nd in the third cycle. If each jump is treated as a separate static measurement, independent fractionation corrected $^{142}Nd/^{144}Nd$ and $^{148}Nd/^{144}Nd$ ratios can be calculated from cycle 2 and cycle 3 respectively. The two measure-

Table 2
Summary of the fractionation and mixing models used.

Fractionation model (Fig. 3)	Mixing model (Fig. 5)
One homogenous infinite reservoir. $^{146}Nd/^{144}Nd = 0.7219$	3 reservoirs of different and temporally variable $^{146}Nd/^{144}Nd$
Constant ^{144}Nd ion beam intensity of 5 V. Evaporation of other Nd isotopes follow fractionation law of choice	Variable reservoir contributions add to a constant ^{144}Nd ion beam intensity of 5 V. Evaporation of other Nd isotopes follow fractionation law of choice
8 s integration time. Counting statistic uncertainty of $a_1a_2a_3/\sqrt{N}$ where a is a random number between 0.99995 and 1.00005, this gives a Gaussian distribution around $1/\sqrt{N}$	8 s integration time. No counting statistic uncertainty employed
Model data corrected using fractionation law of choice and compared with measured data	Model data corrected using fractionation law of choice and compared with measured data

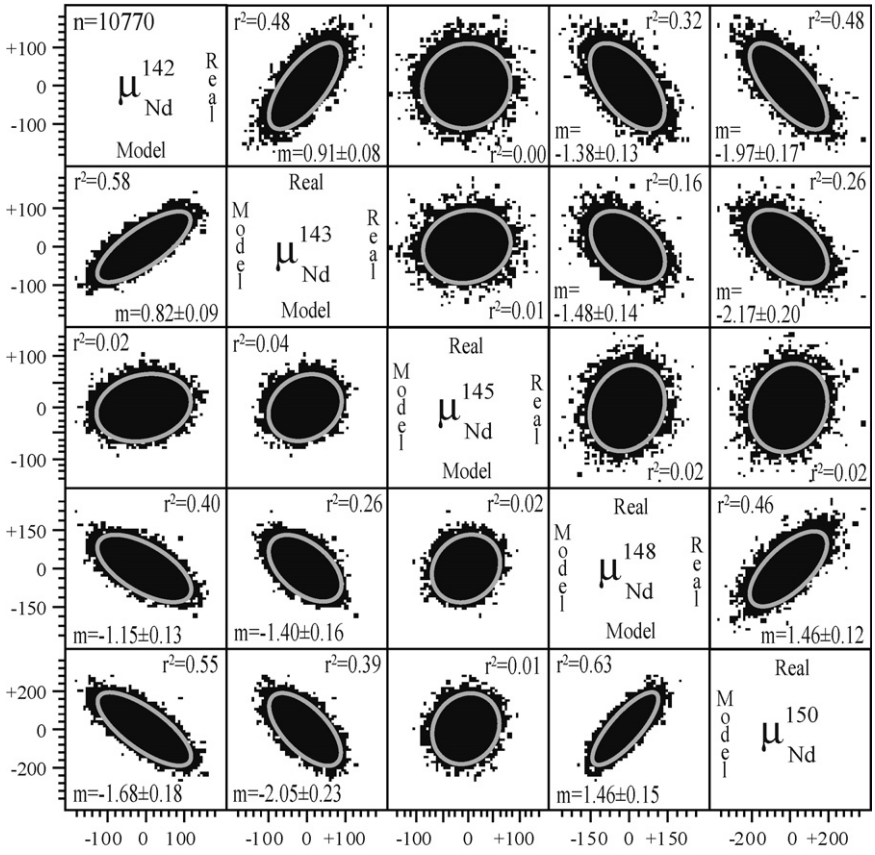

Fig. 3. Correlations between fractionation corrected Nd isotopes, with $\mu^{i}_{Nd} = ({}^{i}Nd/{}^{144}Nd_{CE}/{}^{i}Nd/{}^{144}Nd_{CE} - 1) * 1e6$, where CE is corrected using the exponential law. The upper right panel show all data obtained in Stage 3 (n = 10,770), the lower left panel show modelled data without fractionation, i.e., ${}^{146}Nd/{}^{144}Nd_{M} = 0.7219$. No data rejection has been performed; the ellipses cover 95% of the data. The r^2 value is given for each correlation; the slope of a York-fit linear regression is shown where the correlation is significant, for comparison all slopes are calculated with x as the light isotope and y the heavy. Note the 'mirror' image between real and modelled data.

ments occur 11 s apart (of which 3 s is magnet settling time, 8 s, is peak integration time)—a time span short enough that the fractionation behaviour of a sample is unlikely to change significantly. As these are independent measurements, their uncertainties should be independent, and thus random. Any trend in data must therefore be introduced by the fractionation correction scheme. Fig. 4 shows

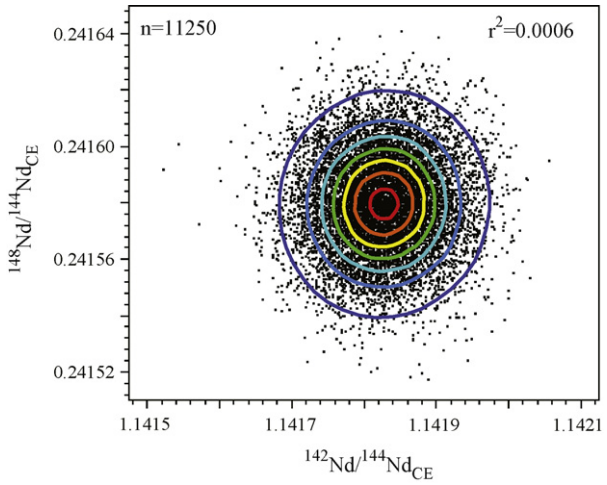

Fig. 4. All ${}^{142}Nd/{}^{144}Nd$ and ${}^{148}Nd/{}^{144}Nd$ ratios (n = 11250) measured statically independent from each other during two different cycles in Stage 2. Both ratios are fractionation corrected using the exponential law. Density ellipses are equidistant from 5% (red) to 95% (dark blue). (For interpretation of the references to color in this figure legend, the reader is referred to the web version of the article.)

the static ${}^{142}Nd/{}^{144}Nd$ and ${}^{148}Nd/{}^{144}Nd$ data (n = 11,250) from the dynamic measurements obtained during Stage 2. The 'shot-gun' pattern is quite different from that exhibited by the μ^{142}_{Nd} vs. μ^{148}_{Nd} data from Stage 3 (see Fig. 3). The correlation in the individual static measurements obtained within dynamic data is absent, and the spacing between the density ellipses is that expected for two independent, normally distributed datasets. The lack of correlation in the independent data strongly suggests that the correlations seen in normal static data are the effects of correlated errors, and that the exponential law is fully capable of correcting for mass dependent isotope fractionation introduced in the source of the thermal ionization mass spectrometer at least for elements with masses and evaporation behaviour similar to those of Nd.

3.1. Exponential law and domain mixing

As discussed above, the exponential law does seem to fully correct for the sample fractionation that occurs during evaporation and ionization in the mass spectrometer source. However, when attempting to resolve isotope anomalies that are very close to the external reproducibility of standard data – for example, ${}^{142}Nd$ anomalies in terrestrial and meteorite samples – it is important that the assumptions on which the chosen fractionation correction is based are valid for both standards and samples. Papanastassiou and Wasserburg [24] calculated that measurable effects in Mg isotopes would result from variable mixing between two domains on the filament. Hart and Zindler [21] found measurable anomalies in an artificial even-abundance Ca isotope mixture and interpreted these anomalies to result from the ion beam representing mixing of different Ca domains in the sample loaded on the filament. More

recently, similar effects have been reported for Nd from analyses of standards displaying non-ideal fractionation [2,22]. Sharma and Chen [2] found that standard data exhibiting reverse fractionation was offset towards higher $^{148}Nd/^{144}Nd$ and $^{150}Nd/^{144}Nd$ compared to those exhibiting normal fractionation. They recommended that to avoid effects from mixing and non-ideal fractionation the data be collected in a narrow window of *F*-values, from −0.1% to +0.1%. Upadhyay et al. [22] found that standards started displaying erratic fractionation behaviour in the later stages of long measurements, leading to elevated $^{142}Nd/^{144}Nd$ and $^{148}Nd/^{144}Nd$ ratios and a slightly depressed $^{145}Nd/^{144}Nd$ ratio towards the end of the standard runs. They interpreted these to be caused by isotope mixing effects and advocated shorter analysis time to minimize creation on the filament of Nd domains of extreme isotopic composition.

The theory of evaporating ionic species in a vacuum [15,16,18] predicts that isotopes of lighter masses evaporate preferentially to those with heavier masses. The measured ratio $^{146}Nd/^{144}Nd$ of the normalizing isotope pair is usually lower than that of the reference $^{146}Nd/^{144}Nd = 0.7219$ at the beginning of a run, and higher at the end of a run; and increases continually for the duration of the run. For the discussion below we call this behaviour *normal* fractionation. The increase in measured $^{146}Nd/^{144}Nd$ can have different functional relationships with time—it may have a simple roughly linear trend, an exponential one, or a trend that is some combination of functions. For some standard runs, a decrease in measured $^{146}Nd/^{144}Nd$ is observed for part of the run, implying that Nd must be evaporating from more than one domain on the filament, each domain having distinct *F*-values. We will call this behaviour *reverse* fractionation. If normal fractionation is observed before a period of reverse fractionation, we will label it as *normal before reverse* fractionation; likewise, if normal fractionation is observed after a period of reverse fractionation, we will label it as *normal after reverse* fractionation. For example, in terms of fractionation, the standard run (depicted in Fig. 5a), block 1 is classified as normal before reverse fractionation; block 2–3, as reverse; and block 4–9 as normal after reverse. For an analysis where $^{146}Nd/^{144}Nd_M$ increases continuously throughout the run (i.e., a positive but not necessarily constant $\Delta F/s$) all data blocks are classified as normal.

If the Nd^+-ions reaching the Faraday Cup collectors come from different domains on the filament, with different isotopic compositions, the assumption of any fractionation law that evaporation occurs from a uniform domain is invalid. This is the case for reverse fractionation, where Nd must come from more than one domain. For normal fractionation, Nd^+-ions could come from one or more domains. Modelling filament domain mixing will not yield unique solutions, as there is no a priori way of finding out the number of domains present, or their isotopic compositions so any modelling of fractionation behaviour is bound to yield non-unique solutions. One can make a few general observations of coupled Nd anomalies as a result of hypothetical domain mixing on a filament. Anomalies introduced by domain mixing are mass dependent; the farther from the normalizing isotopes ^{144}Nd and ^{146}Nd, the larger is the expected anomaly. For instance, ^{150}Nd should show the largest effect; and effects in ^{142}Nd and ^{148}Nd should be nearly identical. The anomalies will always have near constant ratios regardless of the extent of mixing or the degree of fractionation of individual domains. Anomalies in ^{142}Nd, ^{143}Nd, ^{148}Nd, and ^{150}Nd due to domain mixing are positive, while those in ^{145}Nd are negative. Their relative magnitudes, based on a simple mixing models, are $\mu^{142}_{Nd} \cong 2.68\mu^{143}_{Nd}$, $\mu^{142}_{Nd} \cong -8.17\mu^{145}_{Nd}$, $\mu^{142}_{Nd} \cong 1.05\mu^{148}_{Nd}$, and $\mu^{142}_{Nd} \cong 0.36\mu^{150}_{Nd}$ with an uncertainty of 1–2 in the last decimal place of the coefficients.

Reverse fractionation is not observed in any of the rock samples that were analyzed during Stages 1, 2, and 3, but is observed in the standard data reported here, where ~5–8% of the ratios in each stage were obtained during periods of reverse fractionation. Fig. 5a shows the most extreme occurrence of reverse fractionation—from Stage 1, nNdβ-30. The average measured $^{146}Nd/^{144}Nd$ ratio was initially 0.7227, it increased to 0.7234, until the start of block 2, decreased rapidly to 0.7200 during blocks 2 and 3, and then slowly increased (at a constant rate) to 0.7206 through blocks 4–9. The modelling of the $^{146}Nd/^{144}Nd$ ratio assumes a three-domain model of a top, middle, and bottom domain and mixing in time-dependent proportions, first between the top and middle layers, then the middle and bottom layers. The average measured $^{146}Nd/^{144}Nd$ of nNdβ-30 is 0.7209, and the average fractionation corrected $^{142}Nd/^{144}Nd$ is 1.1418284 or $\mu^{142}_{Nd} = +1.2$, making it, on average, a slightly underfractionated standard, run well within the external reproducibility of the standard average. However, when looking at the 9 data blocks of nNdβ-30 (Fig. 5b), it is clear that block 2 exhibits significantly higher $^{142}Nd/^{144}Nd$ and $^{143}Nd/^{144}Nd$ values than the other data blocks. The modelled data show the same trend as the measured data, suggesting that the anomalously high ^{142}Nd and ^{143}Nd values of block 2 are indeed a result of domain mixing. It is interesting that the maximum effect of mixing is seen in block 2, where

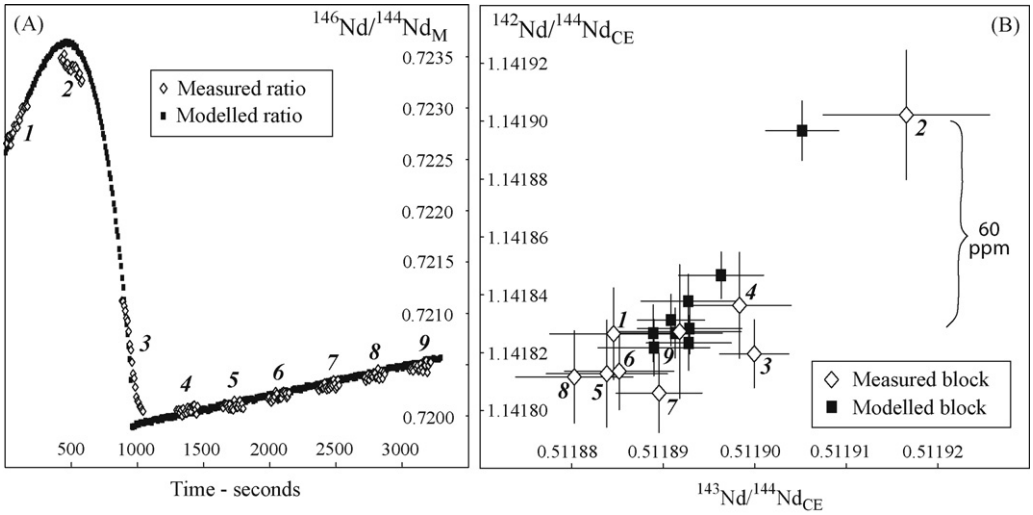

Fig. 5. (A) Measured and modelled variations in $^{146}Nd/^{144}Nd$ with time for standard run nNdβ-30 from Stage 1, which show extreme mixing. (B) Variations in $^{142}Nd/^{144}Nd$ and $^{143}Nd/^{144}Nd$ for the 9 actual and modelled data blocks of nNdβ-30.

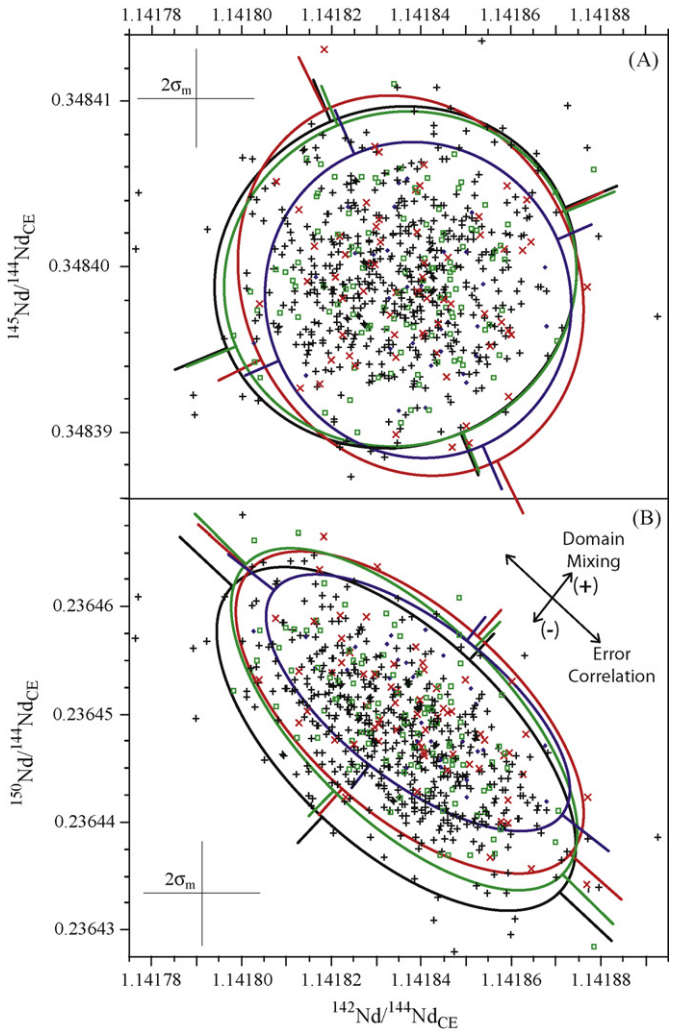

Fig. 6. Degree of correlation during Stage 3 of $^{142}Nd/^{144}Nd$ and $^{145}Nd/^{144}Nd$ (A), and $^{142}Nd/^{144}Nd$ and $^{150}Nd/^{144}Nd$ (B) of the nNd-b standard for 714 individual data blocks collected during Stage 3. Data obtained during normal fractionation (black crosses), reverse fractionation (red crosses), normal after reverse fractionation (green squares), and normal before reverse fractionation (blue diamonds), all data are corrected for mass fractionation using the exponential law. Ellipses covering 95% of the data are shown for 'normal' (black), 'normal before reverse' (blue), 'normal after reverse' (green), and 'reverse' (red) fractionation. Ellipses for normal before reverse and normal after reverse fractionation are identical to that of reverse fractionation. Average $2\sigma_m$ error bars shown, individual error bars omitted for clarity. Also shown in B are the trajectories for the error correlation and for increasing and decreasing amounts of domain mixing. (For interpretation of the references to color in this figure legend, the reader is referred to the web version of the article.)

reverse fractionation yields less variation in $^{146}Nd/^{144}Nd$ than block 3.

The individual isotope ratios collected during Stages 1, 2, and 3, exhibit an interesting pattern. Not only are the data collected during periods of reverse fractionation, on average, slightly higher in μ_{Nd}^{142}, μ_{Nd}^{143}, μ_{Nd}^{148}, and μ_{Nd}^{150} compared to the data obtained during normal fractionation, but so are the data obtained during normal fractionation for standards that exhibited reverse fractionation elsewhere during the run. Fig. 6 show the variations in fractionation corrected $^{145}Nd/^{144}Nd$ and $^{150}Nd/^{144}Nd$ with $^{142}Nd/^{144}Nd$ for the individual data blocks of Stage 3, by fractionation behaviour, similar to the μ_{Nd}^{145} vs. μ_{Nd}^{142} and μ_{Nd}^{150} vs. μ_{Nd}^{142} panels of Fig. 3. There is no difference in the $^{145}Nd/^{144}Nd$ value for a given $^{142}Nd/^{144}Nd$ value for the different fractionation groups. All data ellipses are roughly spherical and coincident; the long axes of the ellipses representing reverse, and normal before reverse fractionated data are almost perpendicular to the long axes of the normal and normal after reverse fractionated data. On the other hand, the $^{150}Nd/^{144}Nd$ and $^{142}Nd/^{144}Nd$ values for normal before reverse, normal after reverse, and reverse fractionated data are all shifted to slightly higher values than those of normal fractionation. This is evident from the parallel, offset long axes, but overlapping short axes. Data obtained under fractionation conditions different than normal fractionation give on average slightly higher $^{142}Nd/^{144}Nd$ and $^{150}Nd/^{144}Nd$ ratios than those obtained for normal fractionation, consistent with larger extents of domain mixing on a filament, during abnormal fractionation. The $^{142}Nd/^{144}Nd$ and $^{150}Nd/^{144}Nd$ ratios are the best suited Nd ratios to examine mixing effects and error correlations as the latter are negatively correlated and the former positively correlated giving almost perpendicular trends, compared to $^{148}Nd/^{144}Nd$ and $^{150}Nd/^{144}Nd$ where both effects give a positive correlation and almost parallel trends.

Comparing the Nd isotope ratios obtained during each of the differing conditions of fractionation shows that reverse, normal before reverse, and normal after reverse fractionated data all differ significantly from those fractionated normally. In Fig. 7, the deviations from normal fractionation are shown along with calculated best-fit mixing models for reverse, normal before reverse, and reverse fractionated data. The data obtained during reverse, normal before reverse, and normal after reverse fractionation show the same extent of mixing, and all show larger extents of mixing than for data obtained during normal fractionation. It is not surprising that data collected during reverse fractionation show effects of mixing, but it is noteworthy that the data collected during normal fractionation, before or after reverse fractionation also show effects of mixing to the same extent, despite not showing any readily visible signs of mixing in their $^{146}Nd/^{144}Nd$ ratios. The effects of mixing on $^{142}Nd/^{144}Nd$ are on the order of ~3 ppm—roughly half of the external reproducibility for all data. This relationship holds true for the other Nd isotope ratios as well, suggesting that domain mixing may be responsible for a significant portion of the external reproducibility. Data obtained during reverse fractionation could, of course, be deemed to definitively exhibit domain mixing and rejected outright, but given that data obtained during normal before reverse, and normal after reverse fractionation show mixing to the same extent, this will not significantly improve data quality. During the analysis of a sample or standard, $^{146}Nd/^{144}Nd$ is only monitored when data are being collected; the fractionation history of the sample or standard is not recorded during the heating of the filament, the focusing and peak centring of the ion beam, the baseline measurements, the gain calibrations of the Faraday collectors, etc. It is therefore very difficult to assess if a particularly sample or standard that showed normal fractionation during data collection, displayed normal fractionation throughout the entire run, or if it experienced a period of reverse fractionation before data collection or approached a period of reverse fractionation after data collection.

Reverse fractionation was not observed for any of the rock samples analysed during Stage 1, 2, or 3, but the speed of fractionation, $\Delta F/s$ was often higher for samples than for standards, making it difficult to estimate whether or not the samples underwent domain mixing to the same extent as the standards to which they were compared. Samples that show higher $\Delta F/s$ might be expected to undergo less mixing than standards. In relation to the standards, such rock samples will display collateral deficits in ^{142}Nd, ^{148}Nd and ^{150}Nd. This in fact, is likely the case for negative ^{142}Nd anomalies reported by us: the Deccan basalt sample BN 016 B of [25] shows the most negative, but not reproducible μ_{Nd}^{142} of −13.3 [9], coupled with μ_{Nd}^{148} and μ_{Nd}^{150} values of −12.4 and −29.6, respectively. These are very close to

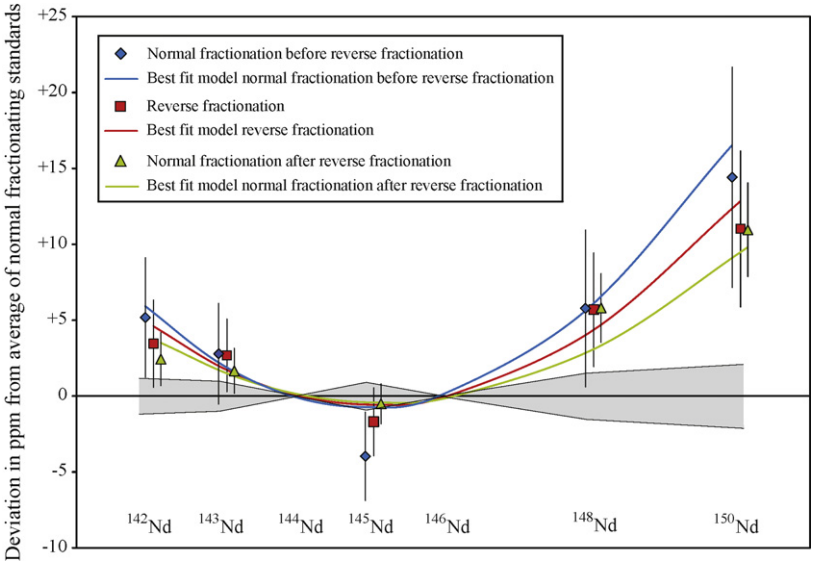

Fig. 7. Part per million deviations from normally fractionated average for reversely fractionated and normal fractionation before and after reverse fractionation for all Nd isotopes during Stage 3, along with best-fit mixing model curves. All error bars are $2\sigma_m$, the shaded area denote $2\sigma_m$ for normally fractionated data.

those predicted by our mixing model: $\mu^{148}_{Nd} = -13.3/1.05 = -12.7$ and $\mu^{150}_{Nd} = -13.3/0.36 = -36.8$, suggesting that negative ^{142}Nd isotope anomalies could be an artefact of domain mixing. Similarly, nine samples exhibiting negative ^{142}Nd anomalies reported by O'Neil et al. [10], also exhibit anomalies in ^{148}Nd and ^{150}Nd of the magnitudes that would be expected if domain mixing is responsible for the anomalies, and are very similar to the non-reproducible anomalies of Deccan basalt BN 016. The average Nd isotopic composition of the faux-amphibolites, felsic band, and tonalites from O'Neil et al. [10] are: $\mu^{142}_{Nd} = -12_{FA}, -10_{FB}, -14_{Ton}$; $\mu^{148}_{Nd} = -13_{FA}(-11), -12_{FB}(-9), -11_{Ton}(-14)$; and $\mu^{150}_{Nd} = -24_{FA}(-31), -31_{FB}(-27), -38_{Ton}(-38)$, where the values in parentheses are those predicted by our mixing model for the given μ^{142}_{Nd} values. These variations are very close ($\sim$2–4σ) to the external reproducibility, so it is statistically possible that the similarity is coincidental, though it is unlikely that *all* the terrestrial samples with measureable negative ^{142}Nd anomalies, also have borderline negative ^{148}Nd and ^{150}Nd anomalies. The samples analysed by Andreasen et al. [9], and O'Neil et al. [10] without ^{142}Nd anomalies, have ^{148}Nd and ^{150}Nd values much closer to those of the standards, than those with the reported negative ^{142}Nd anomalies. If the negative ^{142}Nd anomalies of [10,25] are caused by domain mixing, the standards analysed must on average have larger degrees of domain mixing than the samples exhibiting negative ^{142}Nd anomalies.

As speculated by Upadhyay et al. [22] positive ^{142}Nd anomalies may also result from domain mixing. For example, there is a hint of domain mixing in the dataset of Bennett et al. [7] where the average μ^{148}_{Nd} and μ^{150}_{Nd} of the analyzed Southwest Greenland tonalites are +4.5 and +10.0, respectively. If these positive values were caused by domain mixing, the corresponding increase in μ^{142}_{Nd} would be +4.4, which incidentally is about the offset between the μ^{142}_{Nd} values in the dataset of Bennett et al. [7] and the dataset by Caro et al. [4], whose μ^{148}_{Nd} and μ^{150}_{Nd} values on average are closer to those of the standard. We emphasize that the ^{148}Nd and ^{150}Nd variations in the data of Bennett et al. [7] are well within the reported analytical uncertainty and may not be significant, but again it is intriguing that the most extreme ^{142}Nd anomalies correlate with the highest deviations in ^{148}Nd and ^{150}Nd.

As domain mixing effects are most pronounced for the isotope ratio that is farthest from the ratio used for normalization, using a different isotope pair for fractionation correction that would enhance or suppress these effects should be instructive. We also note that a different normalizing ratio would also affect the overall internal precision of the data, which is mainly controlled by the mass difference between the two isotopes used for normalization. For example, in static measurements where the same amount of time is spent counting each isotope, domain mixing effects will be suppressed and better precision obtained when the normalizing ratios are ^{148}Nd/^{144}Nd or ^{150}Nd/^{144}Nd rather than ^{146}Nd/^{144}Nd. The main drawback of these normalizations is that the domain mixing effects will be enhanced for ^{142}Nd and ^{143}Nd where they are difficult to resolve from radiogenic effects. Alternatively, the data can be normalized using an isotope ratio with ^{142}Nd in the denominator. Fractionation correction using ^{144}Nd/^{142}Nd gives, for the data in Stage 3, results in overall 10% worse precision than using ^{146}Nd/^{144}Nd but more than doubles domain mixing effects in ^{150}Nd. The most precise data is obtained when the data are normalized to ^{146}Nd/^{142}Nd ratio (cf. [17]). For data in Stage 3, this gives about 15% better precision than when using ^{146}Nd/^{144}Nd while increasing any domain mixing effects in ^{148}Nd and ^{150}Nd by about 35%. If this normalization is used for data reduction the relative excesses or deficits in ^{142}Nd in geologic samples with respect to standards will be evident from the correlated anomalies in other stable Nd isotope ratios. Since the other Nd isotopes anomalies change in a linear and predictable manner as ^{146}Nd/^{142}Nd deviates from a "true" value, the presence or absence of anomalous ^{142}Nd can be easily assessed, when normalization is done using ^{146}Nd/^{142}Nd ratio. This indicates that to critically evaluate whether the observed ^{142}Nd anomalies in a data set are real or analytical artefacts the raw data should also be normalized to ^{146}Nd/^{142}Nd ratios and collateral variations in other isotope ratios examined.

4. Conclusions

The exponential fractionation law is fully adequate in correcting for mass dependent isotope fractionation introduced in the TIMS source at the level of presently obtainable precision. This is not the case for other fractionation laws, including the Rayleigh law. Apparent mass dependent correlations between fractionation corrected isotope ratios are correlated errors caused by counting statistic uncertainties. Since these correlations are not related to the fractionation behaviour of the sample, employing additional fractionation correction would not make them disappear. The fractionation behaviour of samples becomes important for

high-precision TIMS data as domain mixing in the standard may account for up to 50% of the external reproducibility. The fractionation behaviour of a sample is not necessarily a good measure of the amount of mixing between domains on the filament. For samples showing reverse fractionation, there appear to be mixing to the same extent before, during, and after the period of reverse fractionation. There is likely significant mixing taking place in samples show only normal fractionation. Reported negative ^{142}Nd anomalies in terrestrial samples are associated with negative anomalies in ^{148}Nd and ^{150}Nd, suggesting these are the product of lesser extents of domain mixing in the 'anomalous' samples compared to the standard. It is imperative to measure *all* isotopes of Nd with the best possible precision and to normalize the raw data using ^{146}Nd/^{142}Nd ratio in order to assess whether the ^{142}Nd anomalies observed using ^{146}Nd/^{144}Nd ratio normalization are real or the products of domain mixing during analysis.

Acknowledgements

Laboratory and mass spectrometer assistance by Patricia Horan, Joanne Donoghue, and in particular Cynthia Chen is greatly appreciated. Eric Posmentier is thanked for stimulating statistics discussions. The manuscript is much improved thanks to a thorough and thoughtful review by Stefan Richter. We are grateful to Dimitri Papanastassiou whose insightful comments helped improve the paper further. This work is supported by the Department of Earth Sciences, Dartmouth College, NSF Grants EAR-0130631 and EAR-0336405 to MS, and Grant 272-07-0015 from the Danish Natural Science Research Council to RA.

References

[1] G. Caro, B. Bourdon, J.L. Birck, S. Moorbath, Sm-146–Nd-142 evidence from Isua metamorphosed sediments for early differentiation of the Earth's mantle, Nature 423 (2003) 428–432.
[2] M. Sharma, C. Chen, Neodymium isotope fractionation in the mass spectrometer and of the issue Nd-142 anomalies in early Archean rocks, Precambrian Research 135 (2004) 315–329.
[3] M. Boyet, R.W. Carlson, Nd-142 evidence for early (>4.53 Ga) global differentiation of the silicate earth, Science 309 (2005) 576–581.
[4] G. Caro, B. Bourdon, J.L. Birck, S. Moorbath, High-precision Nd-142/Nd-144 measurements in terrestrial rocks: constraints on the early differentiation of the Earth's mantle, Geochimica et Cosmochimica Acta 70 (2006) 164–191.
[5] R. Andreasen, M. Sharma, Solar nebula heterogeneity in p-process samarium and neodymium isotopes, Science 314 (2006) 806–809.
[6] K. Rankenburg, A.D. Brandon, C.R. Neal, Neodymium isotope evidence for a chondritic composition of the moon, Science 312 (2006) 1369–1372.
[7] V.C. Bennett, A.D. Brandon, A.P. Nutman, Coupled Nd-142-Nd-143 isotopic evidence for Hadean mantle dynamics, Science 318 (2007) 1907–1910.
[8] M. Boyet, R.W. Carlson, A highly depleted moon or a non-magma ocean origin for the lunar crust? Earth and Planetary Science Letters 262 (2007) 505–516.
[9] R. Andreasen, M. Sharma, K.V. Subbarao, S.G. Viladkar, Where on Earth is the enriched Hadean reservoir? Earth and Planetary Science Letters 266 (2008) 14–28.
[10] J. O'Neil, R.W. Carlson, D. Francis, R.K. Stevenson, Neodymium-142 evidence for Hadean mafic crust, Science 321 (2008) 1828–1831.
[11] M. Sharma, D.A. Papanastassiou, G.J. Wasserburg, R.F. Dymek, The issue of the terrestrial record of Sm-146, Geochimica et Cosmochimica Acta 60 (1996) 2037–2047.
[12] M. Sharma, D.A. Papanastassiou, G.J. Wasserburg, R.F. Dymek, The issue of the terrestrial record of Sm-146—Reply, Geochimica et Cosmochimica Acta 60 (1996) 3751–3754.
[13] M.H. Dodson, A theoretical study of the use of internal standards for precise isotopic analysis by the surface ionization technique: Part I—General first-order algebraic solutions, Journal of Scientific Instruments 40 (1963) 289–295.
[14] W.A. Russell, D.A. Papanastassiou, T.A. Tombrello, Ca isotope fractionation on earth and other solar-system materials, Geochimica et Cosmochimica Acta 42 (1978) 1075–1090.
[15] L. Rayleigh, Philosophical Magazine 42 (1896).
[16] I. Langmuir, The vapor pressure of metallic tungsten, The Physical Review 2 (1913) 329–342.
[17] G.J. Wasserburg, S.B. Jacobsen, D.J. Depaolo, M.T. McCulloch, T. Wen, Precise determination of Sm/Nd Ratios, Sm and Nd isotopic abundances in standard solutions, Geochimica et Cosmochimica Acta 45 (1981) 2311–2323.
[18] K. Habfast, Fractionation correction and multiple collectors in thermal ionization isotope ratio mass spectrometry, International Journal of Mass Spectrometry 176 (1998) 133–148.
[19] D. Vance, M. Thirlwall, An assessment of mass discrimination in MC-ICPMS using Nd isotopes, Chemical Geology 185 (2002) 227–240.
[20] M.F. Thirlwall, Long-term reproducibility of multicollector Sr and Nd isotope ratio analysis, Chemical Geology 94 (1991) 85–104.
[21] S.R. Hart, A. Zindler, Isotope fractionation laws—a test using calcium, International Journal of Mass Spectrometry and Ion Processes 89 (1989) 287–301.
[22] D. Upadhyay, E.E. Scherer, K. Mezger, Fractionation and mixing of Nd isotopes during thermal ionization mass spectrometry: implications for high precision Nd-142/Nd-144 analyses, Journal of Analytical Atomic Spectrometry 23 (2008) 561–568.
[23] K.R. Ludwig, Isoplot, Berkeley Geochronology Center, 2003.
[24] D.A. Papanastassiou, G.J. Wasserburg, Rayleigh distillation constraints on Mg isotopic compositions, Lunar and Planetary Science Conference XVIII (1987) 758–759.
[25] R. Andreasen, K.V. Subbarao, M. Sharma, Nd-142 in Deccan Traps and early mantle differentiation, Geochimica et Cosmochimica Acta 68 (2004) A747–A1747.